Chapter 3

Existence of Griffiths phase and unusual spin dynamics in double perovskite Tb_2CoMnO_6

3.1 Introduction:

The materials that possess both the magnetic and electric orders have received intense research attention globally owing to their potential for practical applications in next-generation spintronic devices [152]–[156]. The coupling among the different order parameters allows one to have freedom of an additional gauge for monitoring one of these order parameters by the other which opens up unprecedented opportunities to achieve new functionalities in such materials [7], [152]–[158]. Hence, an invigorated research attention has been bestowed on discovering such multifunctional materials and there is also an ongoing search for the new mechanisms leading to such coupled order parameters. Particular attention has been given to the magnetic oxides comprising the metal cations and the oxygen anions due to their abundant nature and high stability. Among such materials, the DP compounds having the formula $A_2BB'O_6$ (A= Rare earth ions or alkaline ions; B/B'= transition metal ions) have received tremendous research attention worldwide for their wide span of interesting properties such as near room temperature FM insulating ground state, large MDC, colossal magneto-resistance, giant dielectric constant, magneto-caloric effect, E-type of spin ordering driven ferroelectricity, ASD driven meta-magnetic steps, GP, giant EB, low-temperature RSG, SPC, etc [7]–[10], [105], [122], [153], [159]–[162]. In particular, the co-existence of FM, insulating as well as charge-ordering driven polar behavior observed in most of the DP systems has attracted scientists for their far-reaching technological prospects in real-life applications [7]–[9], [109], [158], [163], [164]. The physical properties of the DPs are profoundly influenced by their B-site structural ordering and their electronic structure [8], [9], [17], [18], [121], [159], [165]. The structure of the perfectly ordered DP is made up of a periodic basic unit comprising two perovskite unit cells (ABO_3 and $AB'O_3$) where the B/B′ ions are alternately positioned at two distinct sites forming a checker board like pattern. The self-ordering of such perfect structurally ordered

DPs requires the differences in the charge states (at least by +2) as well as in the ionic radii of the two B/B′ ions [17], [121], [159]. Conversely, B/B′ ions having similar charge states and/or ionic radii trigger the ASD in the system which is realized as the site exchange among the B/B′ ions [8], [121]. As a matter of fact, the ASD in DPs is known to intensely affect its physical properties, especially its magnetic properties leading to the emergence of various exotic states viz., SG states, GP, EB effects, meta-magnetic transitions, etc [7]–[10], [121], [162]. The ordered DPs exhibit ferromagnetism unlike their end members i.e. ABO_3 and $AB'O_3$ (B/B′=Mn, Co, Ni, etc.) which are usually AFM in nature [9], [16]. The ferromagnetism in such ordered DPs is understood by the 180^0 positive super-exchange interactions between B=Co^{2+}/Ni^{2+} and B′=Mn following the Goodenough-Kanamori rule [16], [88]. However, some Co^{3+}/Ni^{3+}/Mn^{3+} ions creep into the system during the sample preparation which is unavoidable. Moreover, the similar charge states of these B/B′ ions also promote ASD in the system [17], [121], [159]. As a consequence, additional AFM interactions come into play in the system via super-exchange interactions Co^{3+}-O^{2-}-Co^{3+}, Co^{3+}-O^{2-}-Mn^{3+}, Mn^{3+}-O^{2-}-Mn^{3+}, Co^{2+}-O^{2-}-Co^{2+}, Mn^{4+}-O^{2-}-Mn^{4+} [9], [105], [162].

Furthermore, as compared to the most intricately studied La and Y-based DP systems, the DP TCMO is a less explored system [116], [117], [166], and hence, exploring its properties may unravel new interesting magnetic states. Recently, some interesting properties in single crystal and the thin film of TCMO have been reported [117], [166]. The single crystal TCMO shows FM interaction and a large rotational magneto-caloric effect [117]. Whereas the thin film of TCMO established the mixed oxidation state of Co (Co^{2+}/Co^{3+}) and slightly larger transition temperature than that of single crystalline TCMO. The dielectric study also revealed an interesting relaxor glass transition which has been observed above the T_C [166]. However, the detailed magnetic properties and the effect of ASD in TCMO are still less explored. Furthermore, due to some inherent ASD and mixed valence states, it is a partially

ordered sample. In the present work, we have analyzed the detailed magnetic properties of the bulk TCMO. Moreover, we have investigated magnetic ground state by NPD and electronic structure study of TCMO.

3.2 Experimental and Characterizations Details:

The polycrystalline sample of TCMO has been prepared by the conventional solid-state reaction method. Highly pure Tb_4O_7, CoO, and Mn_2O_3 (>99.99%) oxide powder as precursors were taken in exact stoichiometric ratio to prepare the sample. The powder after having an hour of intimate grinding was given the heat treatment at 1000 °C for 24 hours in the air. This powder was re-ground and was again heat treated at 1100 °C for 36 hrs. This was followed by several heating cycles at 1200 °C with intermittent grindings for several days. Thus, the obtained powder was pelletized and sintered at 1300 °C for 36 hours which was followed by a slow cooling rate to reduce the ASD. Powder XRD was recorded in a Rigaku Miniflex II X-ray diffractometer. Rietveld refinement of the XRD pattern was done by FULLPROF suite software. The neutron diffraction measurements were carried out at the Dhruva reactor on a PD2 neutron powder diffractometer (λ=1.2443 Å) in Atomic Research Centre, Mumbai, India. The XPS experiment was carried out at room temperature (300 K) by an Omicron multi-probe surface science system with a monochromatic X-ray source (XM1000) with an Al-Kα line. The system has a hemispherical electron energy analyzer (EA 125). The total energy resolution for the monochromatic Al Kα line with photon energy 1486.70 eV, estimated from the width of the Fermi edge, was about 0.25 eV. The pass energy for survey scan spectra and core level spectra was kept at 50 eV with a step size of 0.5 eV and 30 eV with a step size of 0.05 eV, respectively. Throughout the experiment, the average base pressure was maintained at 5.6×10^{-10} torr. All the magnetization measurements (dc and ac) were performed by the SQUID-VSM) based magnetic property measurement system (Quantum Design-MPMS).

3.3 Result and Discussions:

3.3.1 X-ray powder diffraction:

The Rietveld refinement of the XRD pattern recorded at room temperature (300 K) is shown in Fig. 3.1 which confirms that the sample has been prepared in a single phase without any chemical and/or phase impurity. The well-refined pattern with the $P2_1/n$ space group suggests that the sample was crystallized in a single-phase monoclinic structure. The reduced bond angles ($<180^0$) of Mn-O-Mn and Co-O-Co indicate that significant octahedral distortion is present in the Mn/CoO_6 octahedra which are essentially triggered by the smaller ionic radius of the Tb^{3+} ions. A quantitative measure of such distortion can be estimated by the formula: $\delta=(180°-\Phi)/2$, where Φ is the value of Mn-O-Mn/ Co-O-Co angles [167]. In the present case, the value of δ is found to be ~14.425 which suggests that the system has a significantly large distortion in CoO_6/MnO_6 octahedra.

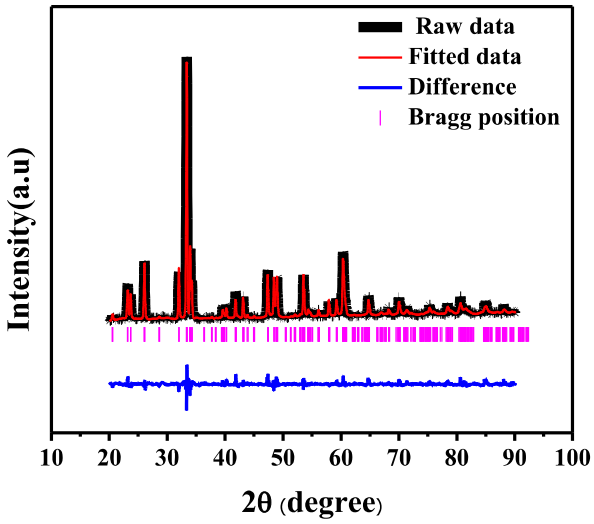

Fig. 3.1: Rietveld refinement of X-ray diffraction pattern at room temperature (300 K).

3.3.2 Neutron diffraction study:

The NPD is an essential tool to probe into the microscopic spin arrangement and structural information of different compounds. Fig. 3.2(a) and (b) show the NPD patterns along with their Rietveld refinement at 300 K and 9 K. All the recorded NPD patterns are successfully refined by the monoclinic phase with space group $P2_1/n$ (14), thus supporting the XRD results. Although, it may be noted that for XRD, both the B-site ions Co and Mn are having similar scattering factors, hence, XRD cannot be taken as a very reliable tool to probe into the cationic ordering for this system [8]. In contrast, for the neutron, different scattering lengths of Co (2.49 fm) and Mn (-3.75 fm) (as well as opposite sign) allow one to estimate the exact occupancies of each atom at each position and also the degree of the B-site cationic ordering [8], [168]. In the present system, refinement shows that the ordering of B-sublattice is around 80% while there exists 20% of ASD. All three oxygen atoms as well Tb-atom have the Wyckoff position of 2e. All the refined parameters including the Wyckoff positions of the atoms, occupancies, bond lengths, etc are shown in Table 3.1. The peak observed at ~19 º is assigned to the (110) reflection. However, on decreasing the temperature below 100 K, we observed a dramatic increase in the intensity of the (110) peak (Fig. 3(c)). Our attempt to refine the NPD patterns only with the nuclear structure $P2_1/n$ resulted in an unsatisfactory fitting. However, the patterns were successfully refined while both the nuclear ($P2_1/n$) and magnetic (P-1) contributions were considered. It is found that the significant contribution to the enhancement of the (110) peak intensity is coming mainly from the magnetic ordering while the contribution from the nuclear structure is merely absent or minimal. The best-fitted refinement of NPD yielded a canted FM type structure as shown in Fig. 3.2(d). The canting of Mn/Co spins is stable down to the lowest measured temperature. In one sublattice Co and Mn are aligned ferromagnetically with each other but canted at some angle with another neighboring sublattice. Similar results

were also observed in an isostructural compound Lu_2NiMnO_6 [169]. The best fit of NPD at 9 K yields the refined moment to be 2.41 μ_B which is lower than the expected complete saturation moment of Co/Mn (3 μ_B). Additionally, the refinement showed the same values of the magnetic moments for both the B-site ions i.e. Co and Mn which is the same as the earlier reported results in similar systems [8], [168], [170]. The temperature variation of the total magnetic moment at Co and Mn sites is demonstrated in the inset of Fig. 3.2(a).

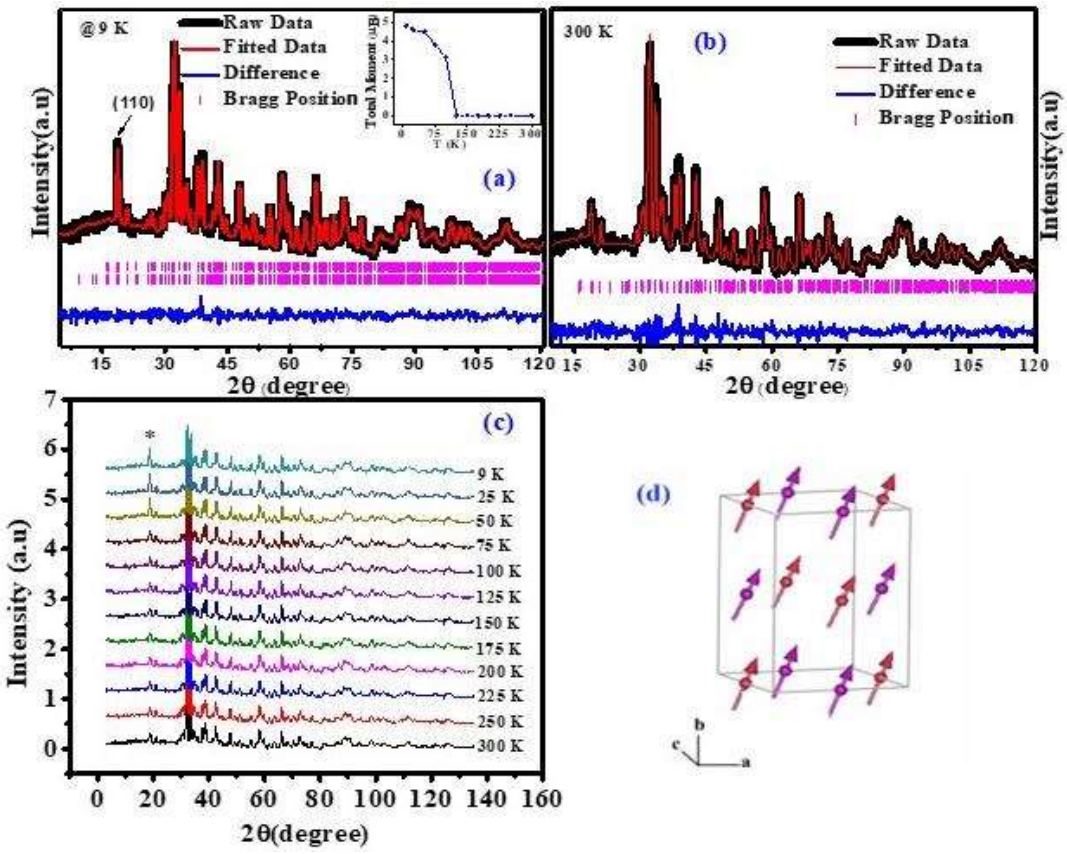

Fig. 3.2: (a) and (b) NPD with its Rietveld refinement at 9 K and 300 K, respectively. Inset of (a): Total moment vs. temperature. (c) Temperature-dependent NPD pattern. (d) Canted FM structure generated from Rietveld refinement of NPD at 9 K, where purple and red arrows denote Co and Mn spins, respectively.

The refined value of the moment is quite close to the theoretically predicted moment for a fully B-site ordered system. This is suggesting that the present system is a highly ordered system. Although, the smaller value indicates the presence of ASD in the system which is also evident from its structural analysis. Due to the existence of ASD Co^{2+}-O^{2-}-Co^{2+} and Mn^{4+}-O^{2-}-Mn^{4+} AFM exchange interactions appear in the system. Moreover, XPS analysis (discussed below) provides information regarding the presence of Mn^{3+}/Co^{3+} ions along with Mn^{4+}/Co^{2+}. These ions also generate additional AFM interactions in the system competing with FM. Thus, the lower value of the refined magnetic moment is associated with the competing AFM and FM exchange interactions arising due to the presence of ASD and mixed valence states of transition metal in the system which is a well-known observation in similar systems [168]–[171]. As a matter of fact, we did not observe any LRO of the Tb ions down to 9 K.

Table 3.1: Structural parameters and crystallographic sites determined from Rietveld profile refinement of the NPD for Tb_2CoMnO_6 at 9 K and 300 K for space group $P2_1/n$.

NPD recorded at	9 K	300 K
β	90.000877	89.98847
a (Å)	5.280563	5.269460
b (Å)	5.560802	5.567892
c (Å)	7.492562	7.493399
V	220.012	219.8543
Tb	4e	4e
x	-0.48399	-0.48281
y	0.56505	0.56492
z	0.25409	0.25503
B_{iso} (Å^2)	0.50759	0.64098
Co	2c	2c
x	0.00000	0.00000
y	0.50000	0.50000
z	0.00000	0.00000
B_{iso} (Å^2)	1.43032	0.63547
Mn	2d	2d
x	0.50000	0.50000
y	0.00000	0.00000
z	0.00000	0.00000
B_{iso} (Å^2)	1.43032	0.63547
O(1)	4e	4e
x	0.40183	0.40308
y	0.96739	0.96878
z	0.24884	0.25050
B_{iso} (Å^2)	0.80744	1.05718
O(2)	4e	4e
x	0.20561	0.20673
y	0.18719	0.19114
z	-0.05088	-0.04719
B_{iso} (Å^2)	0.80744	1.05718
O(3)	4e	4e
x	0.31555	0.31977
y	0.70325	0.70095
z	-0.04901	-0.04974
B_{iso} (Å^2)	0.80744	1.05718
$d_{Co-O(1)}$(Å)	1.96034	1.9495
$d_{Mn-O(1)}$ (Å)	1.94366	1.949
$d_{Co-O(2)}$(Å)	2.08565	2.067
$d_{Mn-O(2)}$ (Å)	1.90932	1.909
$d_{Co-O(3)}$(Å)	2.0466	2.057
$d_{Mn-O(3)}$ (Å)	1.95105	1.952
<(Mn)-(O1)-(Co)>(deg)	147.318	147.881
<(Mn)-(O2)-(Co)>(deg)	147.357	149.201
<(Mn)-(O3)-(Co)>(deg)	147.113	145.912

3.3.2 X-ray Photoemission Spectroscopy Study:

The XPS is a versatile tool to probe the chemical valence states and the ligand coordination of a system. In Fig. 3.3, the XPS survey scan of the system is presented. All the peaks are assigned by the National Institute of standard technology (NIST) confirming the presence of Tb, Co, Mn, and O ions in the system. It also confirms that there are no impurities present in the system other than C. The presence of C is due to its absorption of it by the surface of the sample in the air exposure. The whole analysis has been done after making carbon correction with the C1s line positioned at 284.8 eV to avoid the charging effect error.

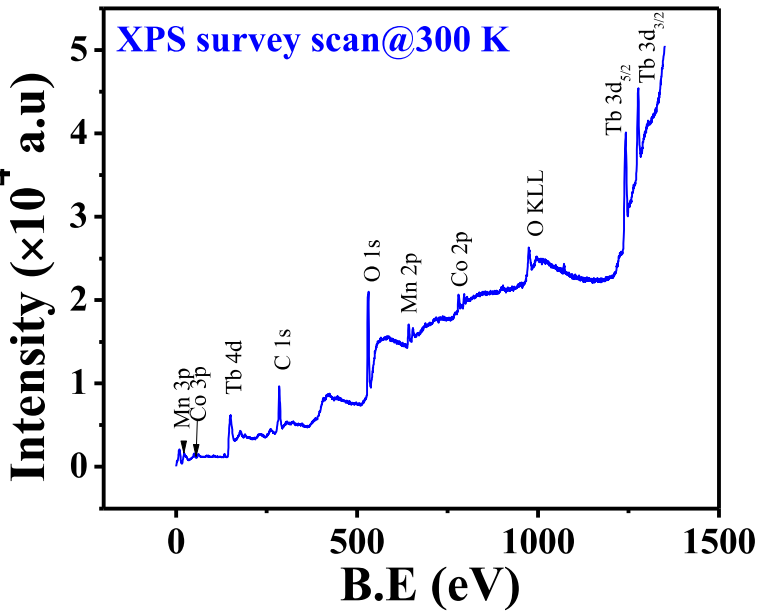

Fig. 3.3: XPS survey scan of TCMO at 300 K.

Fig. 3.4(a) depicts the core level XPS spectra of Tb 3d. It is divided into two major spin-orbit coupling (SOC) peaks $3d_{5/2}$ and $3d_{3/2}$ situated at 1241.3 eV and 1275.8 eV respectively. The values of the peak positions and doublet separation are matched from the NIST database (NIST). The line shape and the peak positions of the Tb3d spectra indicate the trivalent oxidation states for the Tb ions. Fig. 3.4(b) shows the XPS spectra of core level

Mn 2p. The spectra are mainly composed of two main peaks of $2p_{3/2}$ and $2p_{1/2}$ arising due to SOC. The two peaks are positioned at 653.5 eV and 641.7 eV with a doublet separation (DS) of 11.7 eV. In fact, the DS for the Mn2p XPS spectra in MnO_2 is reported to be ~11.8 eV and for Mn_2O_3 is ~11.6 eV (NIST). In our system, observation of the intermediate value of the doublet separation suggests that Mn ions are present in the mixed oxidation states. For further confirmation**,** we deconvoluted Mn2p XPS spectra. As evident from Fig. 3.4(b), the deconvolution analysis suggests the presence of a significant amount of Mn^{3+} ions along with the Mn^{4+} ions. A shake-up satellite peak of $Mn2p_{1/2}$ is clearly visible around 664.6 eV which agrees well with previously reported Mn 2p XPS spectra of a compound having Mn ions in mixed valence states [172]. Further confirmation was sought through the study of the Mn 3s spectra (as shown in the inset of Fig. 3.4(b)) which has the capability of probing the different charge states of Mn precisely. As a matter of fact, the Mn 3s doublet separation is arising due to the exchange splitting (ΔE_{ex}) of the parallel and anti-parallel coupling of a hole in 3d state and electron in a 3s state [173]. Thus, the separation of these two peaks is linearly related to the spin of Mn ions [173], [174]. It is well established that the exchange splitting of Mn 3s spectra is decreased with increased valency of Mn such as it is 4.5 eV for Mn^{4+}, and 5.4 eV for Mn^{3+} [173], [175]. Hence for obtaining quantitative information about the Mn valence state, Mn 3s spectra are important. ΔE_{ex} for the present system is found to be 4.8 eV and we can estimate the Mn valency quantitatively by the linear relation between ΔE_{ex} and ν_{mn} [173], [174]:

$$\nu_{mn} = 9.67 - 1.27\Delta E_{ex}/eV \qquad 3.1$$

Where, ν_{mn} is the Mn valency and ΔE_{ex} is exchange splitting in eV. For our system, the effective oxidation state of the Mn ions comes out to be ~3.57 which is consistent with the Mn 2p spectra results showing mixed valence states.

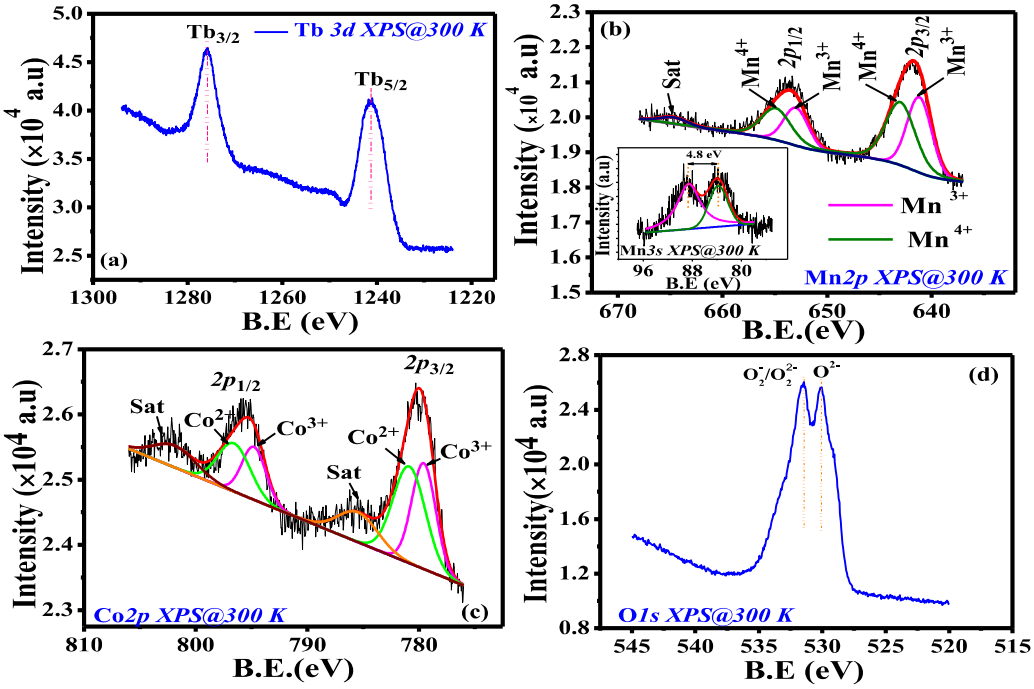

Fig. 3.4: (a) The core level XPS spectra of Tb 3d, (b), (c), and (d) depict the core level XPS spectra of Mn 2p, Co 2p, and O 1s, respectively. Inset of (b) Mn 3s spectra.

The XPS core level spectra of Co 2p are shown in Fig. 3.4(c). The study of core level Co 2p spectra is important as its satellite peaks are very sensitive toward the oxidation states of Co ions. The main photoemission lines in Co 2p XPS spectra are associated with the well-screened states while its satellites are related to the poorly screened states. For CoO where the Co ions exist in divalent states, it shows strong satellite peaks while it is almost absent or relatively feeble in Co_2O_3 or Co_3O_4. Hence, the observation of the clear satellite peaks in the Co2p XPS spectra of the present system indicates the existence of Co^{2+} ions significantly. Apart from this, the reported value of the DS for CoO is 15.9 eV and Co_3O_4 is 15.3 eV [121], [176]. For TCMO, DS of Co2p XPS is found to be ~15.5 eV suggesting the mixed valence states of the Co ions. For further confirmation, the peaks have been

deconvoluted. The deconvolution analysis of the spectra also suggested that both the Co^{3+} and Co^{2+} ions are present in the system.

The O1s XPS spectra are shown in Fig. 3.4(d) Two peaks are observed in the spectra, the first peak positioned at 529 eV is the characteristic feature of O^{2-} ion of lattice oxygen [121] while the other peak at 530.6 eV is ascribed to the less electron-rich oxygen species/absorbed oxygen species (i.e.,O_2^{2-} , O_2^- or O^-) on the surface.

3.3.3. Magnetization study:

In Fig. 3.5(a), the conventional temperature (T) variation of zero field cooled (ZFC) and field cooled (FC) magnetization (M) curves with applied field 100 Oe have been shown. Both the ZFC and FC curves showed an abrupt jump below 100 K suggests the onset of the magnetic ordering in the system. Furthermore, to precisely identify the transition temperature, "dM/dT vs. T" is plotted (the inset of Fig. 3.5(b)). The inflection point of the curve is observed at T_C ~99 K which can be considered the magnetic transition temperature. To further probe the nature of the magnetic transition, we have measured the ac susceptibility (χ). As evident from Fig. 3.5(b), the ac χ' shows sharp and frequency-independent peaks at ~99 K indicating the long-range magnetic ordering. It is pertinent to mention here that the long-range FM ordering is supported by neutron diffraction (discussed above) as it shows the superlattice peak below 100 K moreover the magnetic moment also appears below 100 K and reaches the maximum value at the lowest measured temperature (9 K). Apart from this, the dc ZFC-FC curves also showed a large bifurcation with irreversibility temperature T_{irr}~87 K. Eventually, when a sample is cooled from the high to low temperature, the spins start aligning in the direction of the applied magnetic field or along the energetically favored direction owing to its anisotropy. In the process of ZFC, no field is applied to the sample, therefore the spins are locked in a random direction

in a polycrystalline system according to its anisotropy. Thus, the magnitude of magnetization is dependent upon the anisotropy of the specimen. In the present system, the ZFC curve shows a low value of magnetization while the FC curve starts increasing below the transition temperature and shows a higher value of magnetization (Fig. 3.5(a)) [177]. Hence, this behavior can be attributed to the presence of strong magnetic anisotropy as well as the presence of magnetic spin frustration in the system [178], [179]. We reiterate that the neutron diffraction data also suggest the presence of ASD which leads to the competition between different exchange interactions in the system. This is the basic ingredient for spin frustration in the systems [9], [105], [180]. In the dc magnetization curve, another anomaly is observed below 7 K which can be presumably attributed to the ordering of rare earth elements [10], [119], [181]. Due to the 3d-4f polarization, the magnetic moment of Tb aligns antiparallel with the Co-Mn sublattice. For further investigations of the underlying physics, the ZFC curves have been recorded with the different applied fields (Fig. 3.5(c)). It can be noted that for the lower applied magnetic field, a sharp cusp-like peak is observed which is broadened with an increased magnetic field. Moreover, the peak starts shifting towards a lower temperature with an increasing magnetic field. The maximum temperature of the cusp (T_a) is 98 K at the applied field of 100 Oe and shifts to 95.7 K at 750 Oe. The cusp temperature follows a linear relation with the applied field ($T_a \propto H$) as shown in the inset of Fig. 3.5(c). The spins are frozen due to the competition between the local anisotropy and applied field which results in a cusp-like nature in M_{ZFC}. The local anisotropy is dominated at $T<T_a$ whereas, at $T>T_a$ the applied field is predominated and the crossover occurs when anisotropy energy and the energy due to the applied field become equal [180]. This is a typical field dependence behavior observed in many other systems [179], [182]. Further to confirm the nature of the magnetic transition, the isothermal field-dependent magnetization (M(H)) curves have been recorded

at 95 K and 300 K (Fig. 3.5(d)). The M(H) curve at 95 K shows nonlinear behavior, thus suggesting LRO at this temperature. On the contrary, the M(H) curve recorded at 300 K shows linear behavior suggesting the PM state. Furthermore, to estimate the effective PM moment (μ_{eff}) and CW-Weiss (CW) temperature (θ_{cw}), the standard CW law: $\chi^{-1} = \frac{H}{M} = \frac{3K_B}{\mu_{eff}^2}(T - \theta_{CW})$ was employed to fit the experimental "inverse susceptibility vs. temperature curve" in the PM region (inset of Fig. 3.5(a)). The fit yielded θ_{cw} ~ +34.59 K and μ_{eff} ~ 9.76 μ_B. The positive value of $\theta_{cw,}$ suggests towards the presence of the dominating FM interactions in the system. Furthermore, the large difference between the temperatures θ_{cw} and T_c indicates the presence of AFM interaction along with the dominating FM interaction in the system. The theoretically calculated value of the spin only moment of the system TCMO is found to be 10.65 μ_B (considering all the spins in HS state) which is closely matching with the experimentally obtained effective PM moments.

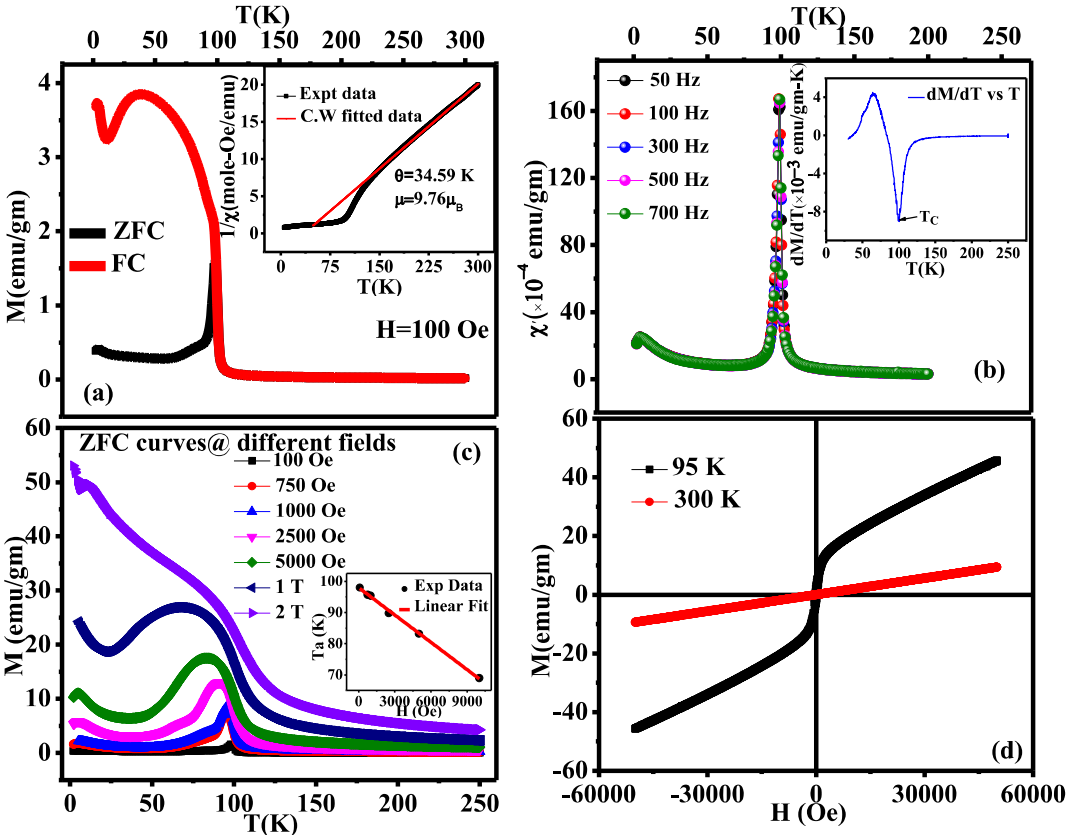

Fig. 3.5: (a) M(T) ZFC-FC curve at 100 Oe for TCMO. The inset presents the "Curie-Weiss fit to the 1/χ vs. T" plot. (b) Ac χ′(T) curves at different frequencies. In the inset of (b) "dM/dT vs. T" plot. (c) "ZFC M(T)" curves at different fields. (d) M(H) curves at 95 K and 300 K.

Interestingly, the temperature variation of the inverse susceptibility study at different magnetic fields showed a peculiar down-turn deviation from the expected linear behavior of the PM state (i.e., violating the CW law) at temperatures well above the magnetic transition temperature $T_c \sim 99$ K (Fig. 3.6). This feature is treated as the signature behavior for identifying GP where a system does not behave like a paramagnet or like a Ferro/anti-ferromagnet [10], [18], [73], [74], [108]. However, on increasing magnetic field, the downturn behavior is observed to get softened and with a sufficiently high field, it yields CW-like behavior, which is also a characteristic feature of GP (Fig. 3.6(a)). The GP

temperature is identified to be T_G ~130 K below which the typical down-turn behavior of the inverse susceptibility curves starts commencing [107], [111], [183].

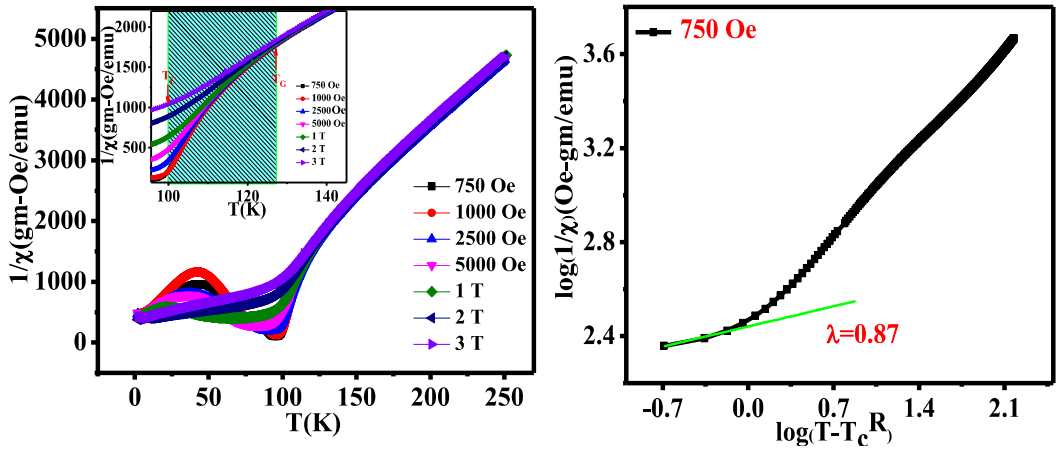

Fig. 3.6: (a)The inverse susceptibility vs. temperature curves at different fields while its inset shows a closer view of the down-turn behavior, (b) The power law fitting to the log-log plot of "$1/\chi$ vs. $((T-T_C^R)/T_C^R)$".

In the GP regime, the susceptibility curves usually follow the power law

$$\chi^{-1} = (T-T_C^R)^{1-\lambda} \qquad 3.2$$

where λ ($0<\lambda<1$) is the power law exponent which is a measure of the deviation from the ferromagnet [73], [74]. In equation (3.2), $\lambda \sim 0$ refers to the CW law in the GP regime and T_C^R is the critical temperature of the randomly diluted perfectly the PM state following the normal CW model. Usually, taking $T_C^R=\theta_{cw}$ is a good choice, since it ensures $\lambda\sim0$ in the PM region. However, systems in which the magnetic ordering temperature (T_c) and CW temperature (θ_{cw}) have a large difference i.e., $\theta_{cw}<<T_c$; putting $T_C^R=\theta_{cw}$ gives errorful estimation of λ. In the present system, there is also a relatively large difference between T_c and θ_{cw} due to the presence of frustration in the system. In such systems, confusion was solved by taking $T_C^R=T_c$ [111]. Fig. 3.6(b) demonstrates the "$\log_{10}(1/\chi)$ vs. $\log_{10}(T- T_C^R)$" plot and its power-law fitting in the linear region of the GP. The fitting yielded $\lambda\sim0.87$

suggesting the presence of GP in the system. Thus, the role of the quenched disorder in the form of ASD may be considered which is known to play a significant role in hindering the LRO and thus leading to the formation of the short-range correlated clusters [184]. Hence, the presence of the ASD in the system which is evident by different analyses as mentioned above may play a significant role in bringing out the GP in the present system by giving rise to random exchange interactions. Additionally, in this system, Co^{2+} and Mn^{3+} ions are J-T active ions which result in the formation of different bond lengths due to crystal field splitting at the e_g level and leaves the system frustrated [185]. Thus, the J-T distortion creates static quenched disorder which may also contribute to the observed GP phase [186]. To further get insight into different magnetic states and how the spin dynamics are affected by the field, we have measured real and imaginary parts of ac susceptibility (χ' and χ'') with different applied dc fields. Fig. 3.7 and its inset are demonstrating χ' and χ'' with frequency at different dc fields. The unusual peaks in χ' have been observed which become broader with increasing the applied field and split into two peaks with further increasing the field.

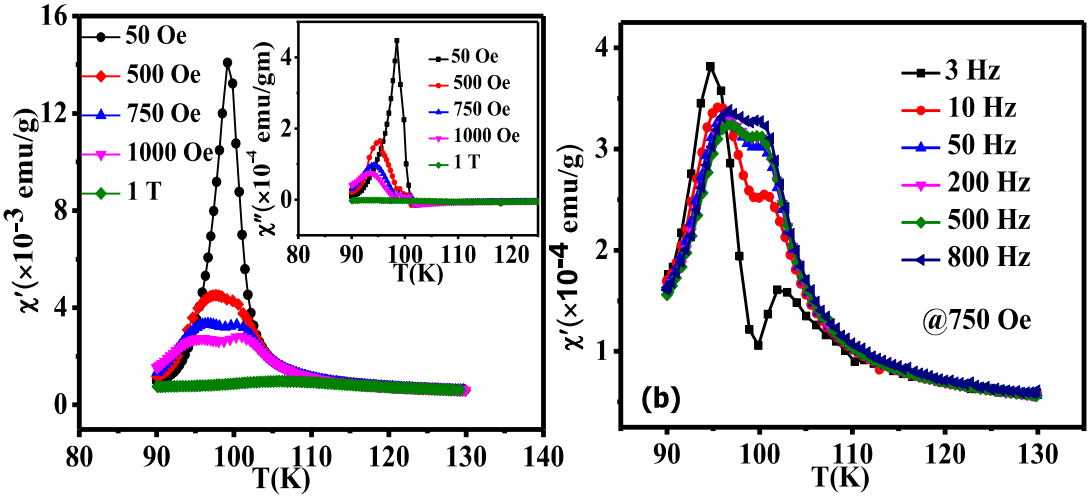

Fig. 3.7: (a) "χ' vs. T" curves at different fields in which peaks become broader with increasing the applied field and split into two peaks as further increases the field, (b) "χ' vs. T" curves at different frequencies recorded with applied dc bias field of 750 Oe.

The peak below T_C shifts towards the lower temperature side with increasing DC bias. On the other hand, the peak at a higher temperature (above T_C) shifts to the higher temperature side with the applied field. In the FM state, the in-phase component χ' can be described as $\chi' \propto \frac{M_S(T)^2}{K(T)}$, where M_S is the saturation magnetization at a particular temperature T and K(T) is anisotropy energy density [180], [182]. The decrease in χ' will result either due to the decrease in saturation magnetization or increase in anisotropy energy. Saturation magnetization does not decrease as the temperature decreases in normal FM material at higher field. Hence decrease in χ' below T_C is due to the increase in anisotropy energy density K [180], [182]. Thus, due to the large anisotropy energy, an additional peak has been observed below T_C as it blocks the spin and does not allow to respond in the magnetic field, this peak is named Hopkinson-like peak [107], [182], [187]. This rapid increase in anisotropy energy below the transition temperature is the result of continuous change in the size and shape of the FM cluster (domain wall motion). Similarly, in the inset of Fig. 3.7, the peak below transition is shifting to the lower temperature side with the field, and the peak at transition or just above the transition suppresses with the application of a higher field. For the typical FM-PM transition, the peak shifts toward higher temperature and suppresses in amplitude with the field (inset of Fig. 3.7), thus this peak is clearly indicating magnetic transition [188]. To further get insight into the origin of this Hopkinson-like peak we performed "χ' vs. temperature" with different frequencies at 750 Oe (Fig. 3.7(b)). We found a very interesting feature in the peak lying immediately below the magnetic transition as it behaves differently for lower and higher frequencies. The peak even at a very low frequency (at 3 Hz) is growing progressively in its amplitude which essentially indicates the unusually slow spin relaxation. This cannot be thermally activated relaxation of a single spin since less frequency dependence has been observed at higher frequencies. The peak is shifting to a higher temperature as increasing the frequency which is quite similar to the

SG state. But suppression in the amplitude of the peak and almost negligible frequency dependence at comparatively high frequencies show strong contrast with the conventional SG phase. Therefore, it rules out the possibility of a SG state. A similar observation of unusually slow relaxation has also been observed earlier in other systems [189], [190]. The underlying physics of such slow relaxation was explained through the existence of oppositely spin-polarized regions arising due to the strong dipolar interactions in such systems [189], [190]. Hence, it is plausible to elucidate the observed similar unusually slow relaxation in the present system by the existence of some oppositely aligned giant domains triggered by the presence of the inherent ASD of this system. Thus, it takes a larger time scale due to the presence of a larger thermal energy barrier while rotating in the direction of the applied field and consequently exhibits slow relaxation showing growth of the associated peak (in χ') even at 3 Hz. It is pertinent here to reiterate that the earlier discussions in the present system disclose the presence of ASD which result in an exhibition of different features such as GP. Thus, the aforementioned origin of the observed slow spin relaxation seems to be plausible for this system. However further theoretical and experimental studies may be helpful to get more insights into the underlying physics of observed phenomena.

3.4. Conclusion:

In this chapter, the structural, magnetic, and electron spectroscopy of TCMO have been investigated. Electronic structure analysis by XPS study reveals the presence of mixed oxidation states (Mn^{4+}/Mn^{3+} and Co^{2+}/Co^{3+}) of B-site ions. The main aspect of the present work is the dc and ac magnetization studies which reveal different interesting phases such as the GP, Hopkinson-like peak, and also unusual slow relaxation in TCMO. The inverse of dc susceptibility shows downturn behavior at low fields which is suppressed with the increase of applied magnetic field indicating the existence of a GP which has been further

confirmed by the power law. The presence of inherent ASD along with mixed valence states of B-site ions and J-T active ions are the most important ingredients for the evolution of this interesting phase. Moreover, the field-dependent ac susceptibility studies unraveled the presence of the Hopkinson peak associated with the domain wall motion and the large anisotropy field. A further study yielded that the relaxation associated with this peak is unusually slow. The different magnetic phenomena observed in the present system have been attributed to the presence of inherent ASD.